Photonic bandgap confinement in an all-solid tellurite glass photonic crystal fiber

Photonic bandgap confinement in an all-solid tellurite-glass photonic crystal fiber

Joris Lousteau,[1] Gerardo Scarpignato,[2] Giorgos S. Athanasiou,[3] Emanuele Mura,[2] Nadia Boetti,[2] Massimo Olivero,[2] Trevor Benson,[3] Phillip Sewell,[3] Silvio Abrate,[1] and Daniel Milanese[2]

[1]*Photonlab, Istituto Mario Boella, Via Pier Carlo Boggio 61, Turin 10138, Italy*

[2]*Photonlab, Politecnico di Torino, Corso Duca degli Abruzzi 24, Turin 10129, Italy*

[3]*George Green Institute for Electromagnetics Research, University of Nottingham, Nottingham NG7 2RD, UK*

**Corresponding author: joris.lousteau@polito.it*

Received September 24, 2012; revised October 21, 2012; accepted October 21, 2012; posted October 22, 2012 (Doc. ID 176664); published November 28, 2012

We report on the fabrication and optical assessment of an all-solid tellurite-glass photonic bandgap fiber. The manufacturing process via a preform drawing approach and the fiber characterization procedures are described and discussed. The fiber exhibits some minor morphological deformations that do not prevent the observation of optical confinement within the fiber by bandgap effects. The experimental fiber attenuation spectrum displays clear bandgap confinement regions whose positions are confirmed by modeling the guiding properties of the ideal geometry using a plane-wave expansion method. The model identifies the bound modes of the structure and provides confirmation of experimentally observed mode field profiles. © 2012 Optical Society of America

OCIS codes: 060.4005, 060.5295, 160.2290, 160.2750.

The unique properties of photonic bandgap fibers (PBF) have made them of interest for numerous application fields [1]. Implementation of PBF for wavelength filtering, chromatic dispersion control, sensing, and nonlinear applications have been demonstrated already and new application fields are to be expected in the near future [2,3]. Up to now, most work has been carried out on hollow-core photonic bandgap fiber (HC-PBF) made from silica glass. The hollow structure, however, presents some disadvantages not only in terms of manufacturing difficulties but also in terms of postfabrication implementation. Actually, basic operations such as fiber cleaving and fiber splicing are technically challenging. As it has been observed for silica glass nanowires [4], long-term degradation of the mechanical and optical properties of the thin glass membranes within HC-PBF also could be a concern.

In terms of glass material, only a limited number of previous papers have reported on PBF made from nonsilica glasses. Among these, one should mention the recent report of a high-quality HC-PBF made from Schott SF6 glass [5]. Composite structures have been developed by pumping tellurite glass or chalcogenide glass into silica microstructured fiber [6,7]. The high thermal-expansion mismatch between these glasses inevitably leads to high mechanical stress, with detrimental effects not only on the mechanical integrity of the fiber structure but also on the refractive index distribution owing to the typically high photoelastic effects occurring in soft glasses [8–10]. In the case of tellurite glass, optical properties would even deteriorate because of the dissolution of silica glass in the tellurite melt [11]. Tellurite glasses present dispersive and nonlinear optical properties that, combined with a PBF structure, could enable the development of optical components of great interest.

To overcome part of these issues, we have manufactured an all-solid tellurite-glass bandgap fiber using all-solid PBF structures discussed by Birks [12] as a general guideline in terms of refractive index and dimensions to design our tellurite-glass PBF.

The fiber was made from two tellurite-glass compositions, namely, TZNGe1 and TZNGe2. The compositions were based on the typical TZN ($TeO_2-ZnO-Na_2O$) [13] glass matrix where GeO_2 was introduced to improve the thermomechanical properties and to reduce the risks of crystallization upon reheating. The glass compositions were designed to have close glass transition temperatures (Tg), and thus close thermal expansion coefficients to prevent mechanical integrity issues. The glass transition temperatures of the two glasses were measured by differential scanning calorimetry (DSC) and were found to be $T_{g1} = 307 \pm 3°C$ and $T_{g2} = 311 \pm 3°C$ for TZNGe1 and TZNGe2, respectively. The refractive index of the TZNGe1 and TZNGe2 glasses was measured by a prism coupling technique at 5 distinct wavelengths: 633, 825, 1061, 1312, and 1533 nm. The results were fitted using the Sellmeier's equation [14]. Taking into account the error on measurements, the so-obtained chromatic dispersion curves of the two glasses were found to be parallel. The difference between the refractive indices of TZNGe2 and TZNGe1 was measured to be $\Delta n = 0.029 \pm 0.001$, and was nearly constant between 633 and 1533 nm.

The fiber was made using the stack-and-draw technique. The tubes and rods used for the preform were manufactured through a combination of rotational casting and stretching techniques, respectively. Thirty-six rods containing TZNGe2 glass were arranged in three rings around a central rod made from the low-index glass TZNGe1. The preform was pulled into 200 m of fiber at a speed of 5 m/min under N_2 atmosphere. The total length of fiber manufactured highlights an additional benefit of relying on a preform drawing approach for manufacturing tellurite-glass PBF. Although the fiber did not show any sign of homogeneous crystallization, localized fiber defects could be observed. As such defects are absent when drawing standard tellurite-glass fiber, we believe that they arise from impurities present in the preform at the interface between the rods.

Figure 1(a) shows an optical micrograph of a cleaved end face of a section of fiber. As one can see in Fig. 1, the

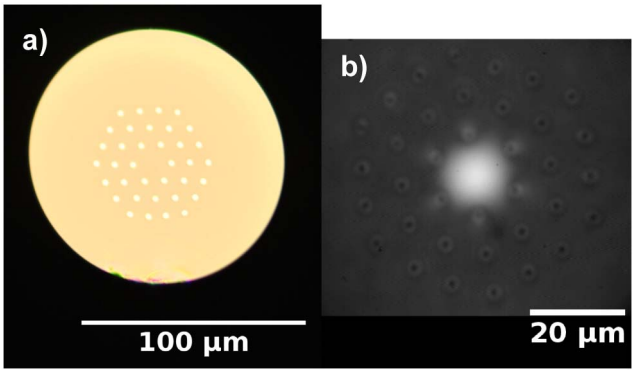

Fig. 1. (Color online) (a) Optical micrograph of the end face of the PBF made from tellurite glass. High-refractive index inclusions from TZNGe2 glass appear bright. The remaining area of the fiber is made from low-index TZNGe1 glass. (b) Near-field output imaging of a 28 cm long section of tellurite-glass PBF shown in (a). The fiber input face was excited in the central low-refractive index area of the fiber using a broadband source spanning from 480 to 2000 nm.

overall hexagonal microstructure is slightly displaced from the fiber center. Also, the shapes of the high-index inclusions, which appear brighter in Fig. 1, are slightly distorted. The origin of these morphological defects is likely to be an air gap existing in the preform between the hexagonal structure and the inner wall of the surrounding tube. This gap, combined with an asymmetrical distribution of the preform temperature, may have led to some deformations with respect to the initial preform structure.

The dimensional characteristics of the fiber are as follows: the mean fiber diameter recorded during drawing was $D_f = 115 \pm 0.5$ μm with maximum fluctuations of ±4 μm over the whole fiber drawing process. The high-index inclusions had a diameter $d = 2.25 \pm 0.20$ μm and the pitch of the microstructured cladding was $\Lambda = 8.6 \pm 0.2$ μm.

Optical assessment of the fiber was performed as described by Bouwmans *et al.* [15]. A commercial supercontinuum source (NKT, SuperK) was focused into a 9 μm core SMF28 optical fiber, which was end-face coupled to the tellurite-glass PBF. The near-field image of the fiber output beam was collected using a Digital DG-03 video camera for visible wavelengths and using a Grunding IR videocamera SN76 IR for longer wavelengths. A near-field IR micrograph of the fiber end face, illustrating guiding in the low-refractive index central region of the fiber, is shown in Fig. 1(b). Either because of the inherent single-mode behavior of the fiber or because of the high attenuation of higher order modes, only the fundamental mode could be observed. The output spectra from the fiber were collected through an iris diaphragm for isolating the beam confined in the low-index central area of the fiber from the nonguided light still propagating through the cladding. Two spectrum analyzers were used, an Avantes model AvaSpec-2048 × 14 for wavelengths ranging from 480 to 1100 nm and a HP70951A optical spectrum analyzer for wavelengths from 700 to 1700 nm.

The initial length of the section of fiber under test was 28 cm. The loss measurements were performed by cutting back successively 11 sections of fiber 1–2 cm long. The fiber output spectra in the visible and in the IR were recorded after each cut to calculate the fiber loss spectrum shown in Fig. 2(a). For each wavelength, the attenuation value was calculated through a linear least square fitting of the experimental data. Typical standard deviation between experimental data and the fitting curve was as high as 4 dB/m.

The cause of such high uncertainty is attributed to the low reproducibility of the end-face cleave quality owing to the difficulty in handling and cleaving the short length of fiber without impairing the optical launching conditions at the input end face of the fiber. Also contributing to the error is the loss measurement procedure, which requires realignment of the output beam with the collecting fiber between each cut. In spite of the care taken, a full reproducibility of the realignment procedure could not be ensured. Nonetheless, the attenuation spectrum in Fig. 2 displays clearly the presence of low-loss guidance for several wavelength bands (clear bands in Fig. 2). For wavelengths within the gray bands shown in Fig. 2, no confinement occurs. At these wavelengths, the low-refractive index central area of the fiber behaves as a highly lossy core from which all light leaks toward the cladding.

The idealized structure, including the Sellmeier fit to experimental refractive index data, was modeled using the commercial Rsoft BandSOLVE software [16], which uses a plane-wave expansion method. Modeling results show that a bandgap exists in the ideal periodic hexagonal lattice over the wavelength range studied (0.4–2 μm). Guided bound modes are not supported by the fiber structure for all wavelengths, however. An overlay to the experimental data given in Fig. 2 indicates those wavelengths for which the model predicted the existence of a clear mode confined by the core defect. In general, the wavelengths for which relatively low loss was observed experimentally are found to closely tally with those for which such a guided bound mode is predicted to exist. The small discrepancy is attributed to the difference between the geometries of the fiber as fabricated and as modeled. The model predicts the continuous existence of a guided bound mode over significant wavelength ranges. In wavelength ranges centered on 740 and

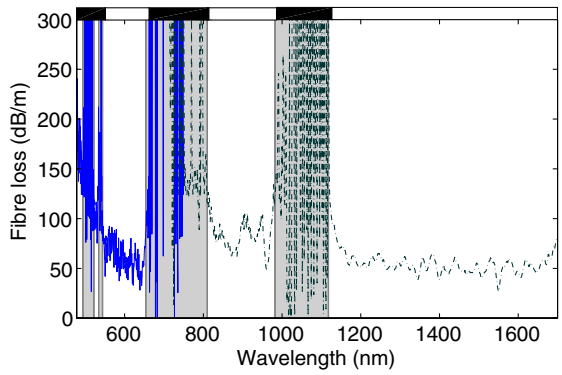

Fig. 2. (Color online) Attenuation spectrum of tellurite-glass PBF measured by cutback technique using a supercontinuum source to illuminate the fiber. Overlay depicts regions where simulations predict guided core-bound modes (white) due to a full photonic bandgap and regions where no guided modes are supported (black).

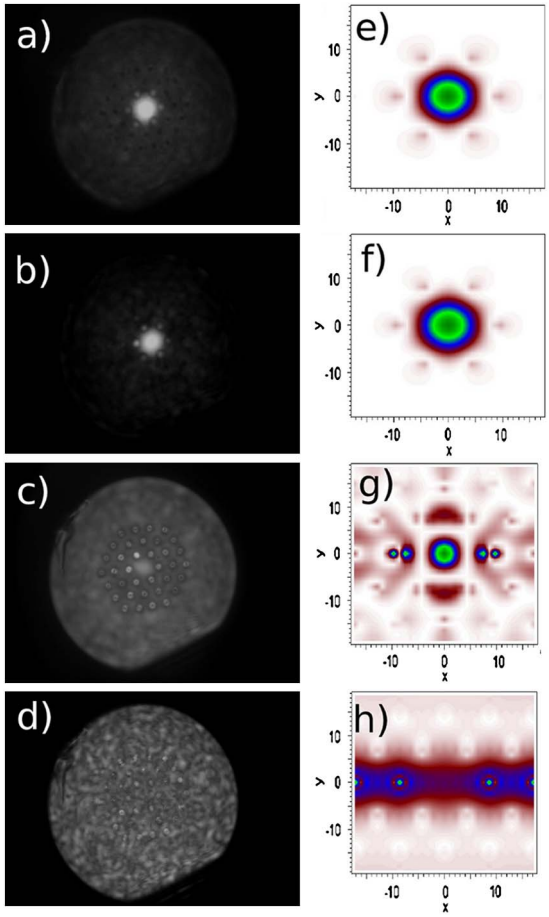

Fig. 3. (Color online) (a)–(d) Experimental near-field photographs of the output of a 28 cm long PBG fiber section made from tellurite glass and taken at wavelengths of 1553, 1300, 980, and 795 nm, respectively. PBF confinement occurred at wavelengths of 1300 and 1553 nm, whereas no confinement was observed at 795 and 980 nm. (e)–(h) Core-hybrid-mode field profiles obtained by modeling the idealized fiber structure at the same wavelengths.

1050 nm, however, the structure supports only unbound (surface) modes. For illustrative purposes, core-bound-mode field profiles obtained for are compared with experimental results in Fig. 3. All these simulation results were confirmed using in-house mode expansion software.

In conclusion, the manufacturing feasibility of an all-solid tellurite-glass PBF, as demonstrated in this Letter, will allow the unconventional properties of tellurite glasses to be combined with those effects associated with bandgap confinement. Actually, the range of refractive index, chromatic dispersion behavior, and transmission properties of tellurite glass, together with the range of fiber geometries achievable, will offer a fine-tuning of the dispersive behavior of this fiber spanning from visible to mid-IR wavelengths. Moreover, an all-solid fiber configuration eases integration with existing optical components and, for instance, offers the possibility to fusion splice tellurite-glass PBF to standard silica glass fiber [17]. To truly exploit this potential, the manufacturing process of tellurite-glass PBF will have to be improved considerably. From glass preparation to fiber drawing, impurity contamination should be reduced drastically. Also, a tellurite-glass PBF structure, including more rings of high-index inclusion glass, would improve the confinement and reduce the losses.

References

1. A. Cerqueira, Rep. Prog. Phys. **73**, 024401 (2010).
2. F. Benabid, Phil. Trans. R. Soc. A **364**, 3439 (2006).
3. V. Pureur, A. Bétourné, G. Bouwmans, L. Bigot, A. Kudlinski, K. Delplace, A. Le Rouge, Y. Quiquempois, and M. Douay, Fiber Integr. Opt. **28**, 27 (2009).
4. G. Brambilla, F. Xu, and X. Feng, Electron. Lett. **42**, 517 (2006).
5. X. Jiang, T. G. Euser, A. Abdolvand, F. Babic, F. Tani, N. Y. Joly, J. C. Travers, and P. St. J. Russell, Opt. Express **19**, 15438 (2011).
6. M. A. Schmidt, N. Granzow, N. Da, M. Peng, L. Wondraczek, and P. St. J. Russell, Opt. Lett. **34**, 1946 (2009).
7. N. Granzow, P. Uebel, M. A. Schmidt, A. S. Tverjanovich, L. Wondraczek, and P.St. J. Russell, Opt. Lett. **36**, 2432 (2011).
8. A. Feltz, W. Burckhardt, B. Voigt, and D. Linke, J. Non-Cryst. Solids **129**, 31 (1991).
9. T. Yano, A. Fukumoto, and A. Watanabe, J. App. Phys. **42**, 3674 (1971).
10. T. Nakai, N. Norimatsu, Y. Noda, O. Shinbori, and Y. Mimura, App. Phys. Lett. **56**, 203 (1990).
11. H. Rawson, in *Inorganic Glass Forming Systems* (Academic, 1967), Chap. 11.
12. T. A. Birks, G. J. Pearce, and D. M. Bird, Opt. Express **14**, 9483 (2006).
13. S. X. Shen and A. Jha, Adv. Mater. Res. **39–40**, 159 (2008).
14. G. Ghosh, J. Am. Ceram. Soc. **7**, 2828 (1995).
15. G. Bouwmans, L. Bigot, Y. Quiquempois, F. Lopez, L. Provino, and M. Douay, Opt. Express **13**, 8452 (2005).
16. RSoft Design, "BandSOLVE," http://www.rsoftdesign.com.
17. H. Li, J. Lousteau, W. N. MacPherson, X. Jiang, H. T. Bookey, J. S. Barton, A. Jha, and A. K. Kar, Opt. Express **15**, 8857 (2007).